Journal of Magnetic Resonance 202 (2010) 14–23

Contents lists available at ScienceDirect

Journal of Magnetic Resonance

journal homepage: www.elsevier.com/locate/jmr

Electron spin relaxation of exchange coupled pairs of transition metal ions in solids. Ti^{2+}—Ti^{2+} pairs and single Ti^{2+} ions in SrF_2 crystals ☆

Stanislaw K. Hoffmann [a,*], Stefan Lijewski [a], Janina Goslar [a], Volodia A. Ulanov [b]

[a] Institute of Molecular Physics, Polish Academy of Sciences, PL-60179 Poznan, Poland
[b] Physical Technical Institute, Russian Academy of Sciences, 420029 Kazan, Russia

ARTICLE INFO

Article history:
Received 5 March 2009
Revised 13 July 2009
Available online 29 September 2009

Keywords:
EPR of Ti^{2+}
Electron spin relaxation
Electron spin echo
Relaxation of dimers
Anti-Orbach relaxation process

ABSTRACT

EPR (X- and Q-band) and electron spin relaxation measured by electron spin echo method (X-band) were studied for Ti^{2+} ($S = 1$) and Ti^{2+}—Ti^{2+} pairs in SrF_2 crystal at room temperature and in the temperature range 4.2–115 K. EPR spectrum consists of a strong line from Ti^{2+} and quartets 2:3:3:2 from titanium pairs ($S = 2$). Spin-Hamiltonian parameters of the pairs are $g_{\|} = 1.883$, $g_{\perp} = 1.975$ and $D = 0.036\ cm^{-1}$. Temperature behavior of the dimer spectrum indicates ferromagnetic coupling between Ti^{2+}. Spin–lattice relaxation of individuals Ti^{2+} is dominated by the ordinary two-phonon Raman process involving the whole phonon spectrum up to the Debye temperature $\Theta_D = 380$ K with spin–phonon coupling parameter equal to 215 cm^{-1}. Important contribution to the relaxation arises from local mode vibrations of energy 133 cm^{-1}. The pair relaxation is faster due to the exchange coupling modulation mechanism with the relaxation rate characteristic for ferromagnetic ground state of the pairs $1/T_1 \propto [\exp(2J/kT) - 1]^{-1}$ which allowed to estimate the exchange coupling $J = 36\ cm^{-1}$. The theories of electron–lattice relaxation governed by exchange interaction are outlined for extended spin systems, for clusters and for individual dimers. Electron spin echo decay is strongly modulated by coupling with surrounding ^{19}F nuclei. FT-spectrum of the modulations shows a dipolar splitting of the fluorine lines, which allows the evaluation of the off-center shift of Ti^{2+} in pair as 0.132 nm. The electron spin echo dephasing is dominated by an instantaneous diffusion at low temperatures and by the spin–lattice relaxation processes above 18 K.

1. Introduction

Solids suitable for EPR and electron spin echo (ESE) measurements of isolated pairs of paramagnetic center are rarely noticed. Isolated pairs of iron group ions appear in some biological materials, where they are separated by large biological molecules [1,2]. Pairs of free radicals appear in photocenters [3,4] and in photoexcited triplet states [5]. The isolated pairs of ions accompany individual ions in some heavily doped dielectric materials like fluorite (CaF_2-type) crystals favorable for dimerization or clusterization of doped divalent metal ions.

The Mn^{2+}—Mn^{2+} pairs were found in BaF_2 [6], in SrF_2 [7] and in CaF_2 [7]. Moreover, Cu^{2+}—Cu^{2+} pairs were observed in BaF_2 [8], Ti^{2+}—Ti^{2+} pairs in CaF_2 [9] and in SrF_2 [9,10], and Yb^{3+}—Yb^{3+} pairs were found in SrF_2 [11]. The electron spin relaxation of exchange coupled pairs was studied for Cu^{2+}—Cu^{2+} in zinc(II)bis(diethyldithiocarbamate) [12], for Cr^{3+}—Cr^{3+} in Al_2O_3 [13], and for Ir^{3+}—Ir^{3+} in $(NH_4)_2PtCl_6$ [14].

Fluorites are cubic crystals (*Fm3m* symmetry, $Z = 4$) with lattice constant $a = 0.58$ nm for SrF_2. Divalent ions introduced into a fluorite lattice are expected to substitute host cations like Sr^{2+}, thus they should be located at the center of SrF_8 cube. However, the difference in ionic radii of host and guest ions and the difference in their electronic structure can produce a local distortion and host lattice relaxation around the impurity ion. Cu^{2+} ions in SrF_2 [15,16] and in BaF_2 [8] are off-center shifted due to Jahn–Teller or pseudo-Jahn–Teller effect [17]. Ti^{2+} ion ($3d^2$, $S = 1$) in the cubic environment has orbitally non-degenerate ground state, thus it is not the Jahn–Teller active ion and off-center shift is not expected. In fact, EPR spectra of Ti^{2+} in SrF_2 [10,18], CaF_2 [9] and $SrCl_2$ [19] consist of a single resonance line indicating the cubic crystal field symmetry at Ti^{2+} located in the center of the $[TiF_8]$ cube. The orbital ground state of Ti^{2+} in a cube of O_h symmetry is an orbital singlet $^3A_2$ with the lowest excited state $^3T_2$ of $\Delta = 6900\ cm^{-1}$ [20]. The EPR line is described by the isotropic g-factor $g = 2.0023 - 8\lambda/\Delta = 1.933$ [10,18] where $\lambda = +60\ cm^{-1}$ is the spin-orbit coupling constant. This line is produced by non-magnetic isotope ^{48}Ti having abundance of 73.72%. The hyperfine splitting appears for magnetic isotopes ^{47}Ti ($I = 5/2$) and ^{49}Ti ($I = 7/2$) having similar nuclear magnetic moments. The hyperfine structure is observed as satellite lines around the central line with splitting 57 MHz ≈ 1.9 mT. Superhyperfine

☆ This paper is written in memory of Dr. Wojciech Hilczer, member of our group, who passed away on 27 November, 2008.

* Corresponding author. Fax: +48 61 8684 52.
E-mail address: skh@ifmpan.poznan.pl (S.K. Hoffmann).

1090-7807/$ - see front matter © 2009 Elsevier Inc. All rights reserved.
doi:10.1016/j.jmr.2009.09.014

interaction with fluorine ligands ^{19}F is too weak to produce a splitting of EPR line and contains isotropic contribution 4.79 MHz ≈ 0.18 mT and anisotropic contribution 2.35 MHz ≈ 0.07 mT as determined from ENDOR measurements [18,20].

Ti^{2+}—Ti^{2+} ($S = 2$) pairs in SrF_2 were identified by their characteristic quartet of lines in the multiline EPR spectrum at low temperatures and their temperature dependence showed that the pairs are ferrromagnetically coupled [18]. In ENDOR studies of the pair in SrF_2 an unusual behavior of fluorine atoms surrounding the Ti^{2+}—Ti^{2+} pairs was discovered [10]. An analysis of angular dependence of the ^{19}F frequencies in the first, second and third coordination spheres showed that one of the fluorine planes surrounded Ti^{2+} is 45° rotated with respect to the host lattice. Thus, a dimer model was proposed as it is shown in Fig. 1. Moreover, it was suggested that instead of homonuclear Ti^{2+}—Ti^{2+} pairs the mixed Ti^{+}—Ti^{3+} pairs can be formed and stabilized by an electrostatic interaction between non-compensated charges leading to a lowering of the local symmetry.

However, not all lines were assigned in the EPR spectra of Ti^{2+} in SrF_2. Thus, we decided to reinvestigate the spectra at X-band and Q-band frequencies at low temperatures. Electron relaxation of Ti^{2+} and its pairs have not been studied at all yet. In this paper we present the results of spin relaxation measurements of single Ti^{2+} ions and Ti^{2+}—Ti^{2+} pairs in SrF_2 crystals. Moreover, we review the results of the previous papers and discuss possible mechanisms and processes of electron spin relaxation of ionic pairs.

2. Experimental

Single crystals of BaF_2 were grown in gaseous helium–fluorine atmosphere by the Bridgman technique as it was described earlier [8,10]. Titanium was introduced into a melt as TiF_4 compound in conditions of fluorine excess. The total concentration of Ti^{2+} ions was estimated by EPR as 2.7×10^{18} ions/g with of about 40% of ions coupled into dimeric species.

Pulsed EPR experiments were performed with a Bruker ESP 380E FT/CW spectrometer with dielectric TE_{011} resonator in the temperature range from 4.2 K to 115 K using flow helium Oxford CF935 cryostat. Above this temperature range the electron spin echo signal was too weak to be detected.

Pulsed experiments were performed on individual titanium ions and on titanium pairs with the external magnetic field along the C_4 crystal axis. Spin–lattice relaxation time T_1 was measured by electron spin echo using the saturation recovery method. The saturating 32 ns pulse having excitation band 1.32 mT was able to excite a single resonance line of monomeric center, whereas the 64 ns pulse (excitation band 0.66 mT) was used for the saturation of a selected dimer line. The magnetization recovery was monitored by the Hahn-type spin echo signal amplitude excited by pulse sequence 16–144–16 ns for single ions and 48–144–48 ns for dimers. The recovery was single exponential in the whole temperature range. Dephasing time T_M was determined from the two-pulse echo decay with the same two-pulse sequences as in T_1 measurements. The exponential decay was strongly modulated by weak dipolar interactions with surrounding ^{19}F nuclei.

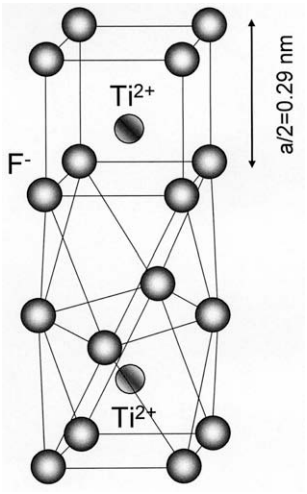

Fig. 1. Model of Ti^{2+}—Ti^{2+} center in SrF_2 crystal according to the ENDOR results [13]. The cubic unit cell dimension is $a = 0.58$ nm.

3. Results and discussion

3.1. EPR of single Ti^{2+} ions and Ti^{2+}—Ti^{2+} pairs in SrF_2 crystal

X-band EPR spectrum recorded at low temperatures with external magnetic field along the C_4-axis is shown in Fig. 2. At $T = 40.6$ K the spectrum is dominated by the single line from Ti^{2+} ($S = 1$) marked by an asterisk. This line was excited during spin echo experiments.

The ^4F term of Ti^{2+} in cubic symmetry O_h is split into a singlet ground state A_2 and two excited triplets T_1 and T_2. In a lower symmetry the excited orbital states are split as it is shown in Fig. 3 for D_{4h} symmetry. The ground state of titanium pairs ($S = 2$) coupled by isotropic exchange $H_{ex} = JS_1 \cdot S_2$ is split into three levels, which are further split by the tetragonal crystal field (zero-field splitting D). When $h\nu > D$ the EPR spectrum consists of four lines with the intensity ratio 2:3:3:2, as it is shown in Fig. 3. The dimer lines at 9 K are marked by arrows in Fig. 2. The three dimer quartets are expected along C_4-axis. One quartet with $2D$-splitting is due to dimers having z-axis parallel to the C_4, whereas two quartets with D-splitting arise from perpendicularly orientated dimers. The amplitude of the dimeric lines grows with lowering of temperature indicating a ferromagnetic coupling in the Ti^{2+}—Ti^{2+} pairs.

The dimer spectrum was described with the spin-Hamiltonian

$$H = \frac{1}{3}b_2^0 O_2^0 + \frac{1}{60}b_4^0 O_4^0 + \frac{1}{60}b_4^4 O_4^4 + g_{\parallel}\mu_B B_z S_z + g_{\perp}(B_x S_x + B_y S_y) \quad (1)$$

with parameters listed in Table 1, together with data for Ti^{2+}—Ti^{2+} pairs in CaF_2 [9].

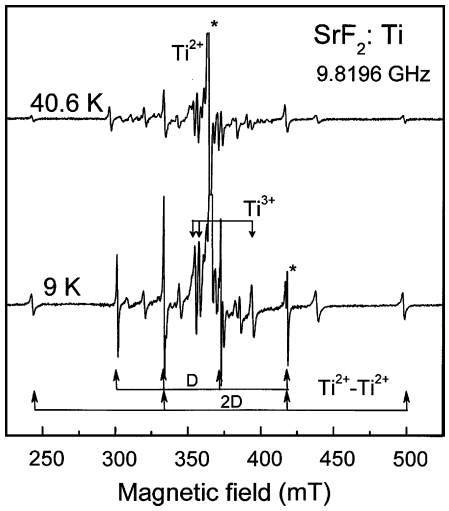

Fig. 2. X-band EPR spectra of titanium ions in SrF_2 at low temperatures with external magnetic field along C_4-axis. The lines of dimeric Ti^{2+}—Ti^{2+} species are split by $2D$ at parallel orientation and by D in perpendicular orientation and are marked by arrows at spectrum 9 K. The asterisks mark lines for which pulsed EPR experiments were performed.

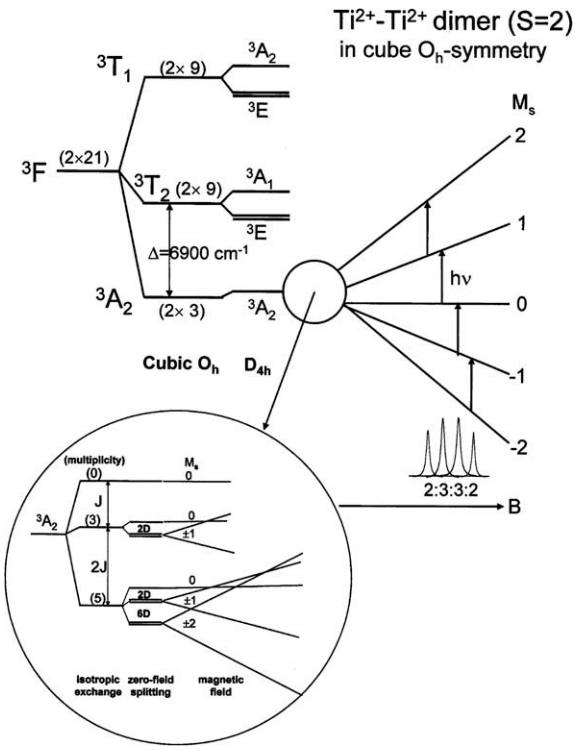

Fig. 3. Energy levels for titanium pairs in axial crystal field symmetry D_{4h} with isotropic exchange J and zero-field splitting D.

The g-factors ($g_{\parallel} = 1.883$ and $g_{\perp} = 1.975$) reflect an axial (tetragonal) deformation of the fluorine cube around the Ti^{2+} in the pair. It means that contrary to the single Ti^{2+} ions, the titanium ions forming dimers are not located at the center of the fluorine cube, but are off-center shifted along the C_4-axis. Zero-field splitting parameter $D = b_2^0 = 3B_2^0 = 0.036\ \mathrm{cm}^{-1}$ is much lower than the microwave quantum at Q- and X-band.

Beside the single lines from cubic Ti^{2+} centers and quartets from dimeric Ti^{2+}—Ti^{2+} species, the lines from a rhombic titanium center were identified. They are plotted by dashed lines in angular dependence of the spectrum at Q-band (Fig. 4). The rhombic spectrum has g-factors: $g_x = 2.035$, $g_y = 1.999$ and $g_z = 1.805$ with the z-axis parallel to the C_4-axis. This spectrum can be assigned to Ti^{3+} ($S = 1/2$) ions substituting Sr^{2+} with additional fluorine ions located in an interstitial position for compensation of excess charge of the Ti^{3+} ion. Thus, this center can be marked as "Ti^{3+}—$F_{interst}$". We did not measure a spin relaxation for this center. It should be mentioned that still some lines remain non-identified in the spectrum.

3.2. Spin–lattice relaxation of single Ti^{2+} ions

Electron spin relaxation of iron group ions in solids can be driven by various mechanisms and processes [21,22]. The relaxation rate $1/T_1$ of Ti^{2+} in SrF_2 increases more than four orders of magnitude in the temperature range 20–100 K as it is shown in Fig. 5,

Table 1
Spin-Hamiltonian parameters (in cm^{-1}) of Ti^{2+}—Ti^{2+} pairs ($S = 2$) in SrF_2 [18] and CaF_2 [9] crystals.

Crystal	$D = \lvert b_2^0 \rvert$	b_4^0	b_4^4	$g_{\parallel}$	$g_{\perp}$
SrF_2	0.036	0	8×10^{-4}	1.883	1.975
CaF_2	0.045	-1×10^{-4}	13×10^{-4}	1.909	1.975

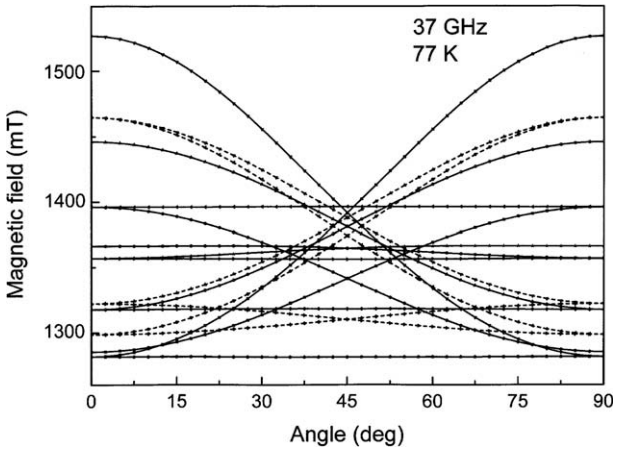

Fig. 4. Angular dependence of the Q-band (37 GHz) EPR spectrum at liquid nitrogen temperature. The solid lines are theoretical plots for Ti^{2+}—Ti^{2+} dimers with parameters listed in Table 1. Dashed lines are plots for monomeric Ti^{3+} center.

where the relaxation results are collected. Such a fast acceleration of the relaxation with temperature can be attributed to the Raman two-phonon relaxation processes involving the whole phonon spectrum, and it is described by the relation

$$1/T_1 = c \cdot T^7 I_6(\Theta_D/T) \tag{2}$$

where the I_6 is the transport integral over the Debye phonon spectrum with Debye temperature Θ_D. The numerical approximation of the I_6 is given in Appendix A. A good computer fit with Eq. (2) can be obtained, but with $\Theta_D = 297$ K which is much lower than the calorimetric Debye temperature $\Theta_D = 380$ K [23]. We addressed this problem in our recent paper [24], where we showed, that except for the Raman process the local mode vibrations contributed to the spin relaxation. In such a case the temperature dependence of $1/T_1$ is described by the following equation

$$\frac{1}{T_1} = a + c \cdot \frac{T^7}{\Theta_D^{10}} I_6(\Theta_D/T) + d \cdot csch^2\left(\frac{E_{\text{local mode}}}{2kT}\right) \tag{3}$$

The first term is a temperature independent contribution influencing relaxation when non-uniform distribution of ions exists in a crystal [25,26]. This contribution can dominate at low tempera-

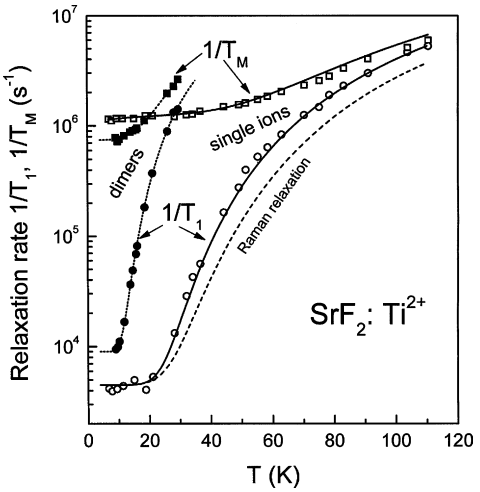

Fig. 5. Temperature dependence of the spin–lattice relaxation rate $1/T_1$ and phase relaxation rate $1/T_M$ for single Ti^{2+} ions and Ti^{2+}—Ti^{2+} dimers in SrF_2. The solid lines are fits to the equations defined in the text.

tures, increases with ion concentration and usually becomes appreciable for concentrations larger than of about 10^{17} ions/g. The last term describes relaxation via local mode of energy $E_{\text{local mode}}$. This term can be approximated by exponential dependence at low temperatures where $kT \ll E_{\text{local mode}}$, and tends to $1/T_1 \propto T^2$ at high temperatures. The Raman process for non-Kramers ions is described by the second term. The best fit to experimental points with parameters: $a = 4500\ \text{s}^{-1}$, $c = 2.3 \times 10^{16}\ \text{s}^{-1}\text{K}^3$, $d = 1.5 \times 10^6\ \text{s}^{-1}$ and $E_{\text{local mode}} = 133\ \text{cm}^{-1}$, is shown as a solid line in Fig. 5. Both the a-term and Raman term produce temperature dependence shown by a dashed line indicating substantial local mode contribution. The d-coefficient of the local mode can be treated as a frequency of the $E_{\text{local mode}}$ barrier crossing. This is order of MHz typical for a tunneling motion through a potential barrier.

The c-coefficient describing the Raman process is [21]

$$c = \frac{9\hbar^3}{4k^3}\left(6\pi^{11/10}\frac{pN_A}{M}\rho^{2/5}\right)^{10/3}\frac{\left|\left\langle s_1|V^{(1)}|s_2\right\rangle\right|^4}{\Delta_{\text{cryst}}^2} \tag{4}$$

where k is the Boltzmann constant, $p = 3$ is the number of atoms in SrF_2 molecule, N_A is the Avogadro number, $M = 126$ g is the molecular weight, $\rho = 4.24\ \text{g/cm}^3$ is the crystal density and $\Delta_{\text{cryst}} = 6900\ \text{cm}^{-1}$ [23] is the orbital splitting shown in Fig. 3. The matrix element $\langle s_1|V^{(1)}|s_2\rangle$ is the spin–phonon coupling parameter describing coupling of the two spin states s_1 and s_2 to phonons modulating crystal field potential. The $V^{(1)}$ is the linear term in the expansion of the crystalline field potential V in the power of fluctuating strain ε produced by phonons $V = V^{(0)} + V^{(1)}\varepsilon + V^{(2)}\varepsilon_1\varepsilon_2 + \cdots$. The experimental value of c-coefficient allows an evaluation of the spin–phonon coupling parameter $\langle s_1|V^{(1)}|s_2\rangle$ as equal to 215 cm^{-1}.

3.3. Electron spin–lattice relaxation of condensed paramagnets-outline of theoretical approaches

An exchange interaction can hardly ever be a direct mechanism of the relaxation. In condensed paramagnets where paramagnetic ions are coupled by dipolar and exchange interaction, the relaxation mechanism is delivered by exchange modulation of the dipolar coupling. In some low symmetry clusters of ions the direct exchange can couple states having the same total spin thus it can produce the relaxation transitions. In dimers of ions exchange acts as a relaxation mechanism in a second-order involving anisotropic interactions. The details are shortly described below.

3.3.1. Relaxation in paramagnets

The exchange interaction dominates the spin–lattice relaxation in paramagnetic solids with relaxation rate much faster than that in magnetically diluted solids. The exchange coupling is usually larger or compared to the Zeeman and dipolar energy and modulates the dipolar interaction. The situation is analogous to the exchange narrowing of homogeneously broadened EPR lines with $T_1 = T_2$. This can be described in a three-bath model containing Zeeman energy, exchange energy and lattice energy. When the direct relaxation of Zeeman energy to the lattice is relatively slow, then the spin excitation energy is first transferred to exchange reservoir by spin–spin interactions. The exchange can be treated as an independent intermediate exchange reservoir which relaxes more rapidly than the Zeeman subsystem and determines experimental value of T_1. Such a relaxation, which can be called a spin–exchange–lattice relaxation was considered in detail in papers [27,28] with results shortly described below.

Assuming that each pair of exchange coupled spins relax independently the total exchange Hamiltonian with summation over pair-wise interaction is

$$H_{\text{ex}} = \sum_{jk} J(x_{jk}) S_j \cdot S_k \tag{5}$$

where jk denotes an adjacent pair of spins.

The Hamiltonian can be expanded in a series $H_{\text{ex}} = H_0 + H_1 + H_2 + \cdots$.

$$H_0 = J\sum_{jk} S_j \cdot S_k \tag{6}$$

$$H_1 = \sum_{jk} S_j \cdot S_k \sum_s \left(\frac{\partial J(x_{jk})}{\partial x_{jk}^s}\right) \cdot u_{jk}^s \tag{7}$$

$$H_2 = \sum_{jk} S_j \cdot S_k \sum_{rs} \left(\frac{\partial^2 J(x_{jk})}{\partial x_{jk}^r \partial x_{jk}^s}\right) \cdot u_{jk}^r u_{jk}^s \tag{8}$$

where x_{jk} is a vector joining adjacent spins; u_{jk} is a small departure of x_{jk} from the equilibrium value, and the superscripts r and s denotes Cartesian components of x_{jk} and u_{jk}.

The H_0 is an isotropic exchange regarded as the unperturbed exchange Hamiltonian. The isotropic exchange Hamiltonian commutes with S and S_z. Therefore, modulations of J of every pair can lead to the transitions where these quantities are conserved and relaxation spin-flops between Zeeman levels cannot appear. Modulation of isotropic exchange can relax spins as a second-order effect only as it will be considered below.

The H_1 and H_2 are perturbations connecting exchange system with lattice vibrations and give finite probability of spin-flop relaxation transition. Assuming that the different pairs of spins contribute in an uncorrelated [27] or correlated [28] manner to the exchange–lattice relaxation process the relaxation rate has been calculated for the direct (single phonon) and for the Raman (two-phonon) processes. In the direct process the H_1-perturbation is involved and the relaxation rate $1/T_1$ varies linearly with temperature as

$$\frac{1}{T_1} = \frac{Z\hbar}{6\pi k^3}\frac{NVa^2}{M}\left(\frac{6\pi^2 N}{V}\right)^{5/3}\frac{J^2}{\Theta_D^3}\left(\frac{\partial J(x_{jk})}{\partial x_{xj}}\right)^2 T \tag{9}$$

where N is the number of molecules, Z is the number of the nearest neighbor sites, thus $N \cdot Z/2$ is the number of separate pairs of spins, V is the volume of the crystal, a is the distance between adjacent spins, M is the atomic mass and k is the Boltzmann constant. The Debye model of lattice vibrations was assumed with Debye temperature Θ_D.

In two-phonon Raman processes the H_2-perturbation is involved and the relaxation rate $1/T_1$ strongly varies with temperature as

$$\frac{1}{T_1} = \frac{12\pi^2\hbar^3[S(S+1)]^3}{5kM^2}\left(\frac{Na}{V}\right)^3 J^2\left(\frac{\partial^2 J(x_{jk})}{\partial x_{jk}^2}\right)^2 \frac{T^9}{\Theta_D^{12}}\int_0^{\Theta_D/T}\frac{x^8 e^x}{(e^x-1)^2}dx \tag{10}$$

with an integration over Debye-type phonon spectrum described by the transport integral I_8 [29,30]. If crystal data are available, then the only unknown parameters in Eqs. (9) and (10) are $(\partial J/\partial x)$ and $(\partial^2 J/\partial x^2)$. These parameters describe a variation of exchange integral with distance and are analogs of the spin–phonon coupling parameter $\langle s_1|V^{(1)}|s_2\rangle$ of ordinary Raman process (see Eq. (4)). The J decreases much more rapidly than the dipolar interaction, and generally depends on an overlap of the atomic orbitals on an exchange pathway [31]. The distance dependence can be approximated by the inverse power law $J \propto x^{-n}$ with $n = 8$–32 depending on the system. A better approximation based on a large collection of experimental data is an assumption that exchange interactions decrease exponentially with the distance as $J \propto \exp(-\lambda|x_{jk}|)$. For large J value it was found $|J| = 1.35 \cdot 10^7 \exp(-1.8x)$, whereas for $J < 0.1\ \text{cm}^{-1}$ $|J| = 5.9\exp(-0.335x)$ [35]. Then $(\partial J/\partial x_{jk}) = \lambda J$ and

$(\partial^2 J/\partial x_{jk}^2) = \lambda^2 J$ and Eqs. (9) and (10) can be parameterized to the form:

$$\frac{1}{T_1} = c_1 \lambda^2 J^4 T \quad \text{for direct process, and} \tag{11}$$

$$\frac{1}{T_1} = c_2 \lambda^4 J^4 T^9 I_8(\Theta_D/T) \quad \text{for Raman process.} \tag{12}$$

The above equations show that the relaxation rate $1/T_1$ strongly depends on the exchange interaction and grows as J^4 in a paramagnetic state of magnetically condensed solids.

In magnetically diluted solids, where pairs or oligomeric species can coexist with individual spins, a situation seems to be simpler, and more detailed information can be obtained from experimental measurements.

3.3.2. Relaxation in triads and tetramers

For triads of paramagnetic ions or for tetramer species with negligible intermolecular dipolar coupling the isotropic exchange coupling can be a direct mechanism of a spin relaxation when transitions fulfilling the selection rules $\Delta S = 0$ and $\Delta M = 0$ are possible. In pairs and in symmetric triads only one total spin state with a given value of S exists and isotropic exchange cannot produce relaxation transitions. In low symmetry trimers, tetramers or larger clusters more total spin states with the same value of S can exist leading to a very effective spin relaxation.

Assuming a triad with $J = J_{13} = J_{23}$ and $J' = J_{12}$ the exchange Hamiltonian can be written as [32,33]

$$H = J(S_1 \cdot S_3 + S_2 \cdot S_3) + J' S_1 \cdot S_2 \tag{13}$$

and energies are $E(S, S') = J \cdot S(S+1)/2 + (J' - J) \cdot S'(S'+1)/2$, where $S' = S_1 + S_2$ and $S = S' + S_3$. The energy levels for symmetric triads (C_{3v}) and for distorted triads (C_{2v}-symmetry) with $J' = 0.5J$ are shown in Fig. 6. Transitions allowed by the exchange can be induced for the distorted configurations only, as it is shown by arrows in Fig. 6. The relaxation of triads has been considered in [25] and detailed calculations were performed for Cr^{3+} triads in ruby [34,35]. Relaxation of tetrads of iron ions has been experimentally studied for [4Fe–4S] ferrodoxin ([36] and see discussion in [[32, p. 133]]).

3.3.3. Relaxation in dimers

An isotropic exchange cannot be a mechanism of spin–lattice relaxation in the first order in dimeric species. However, a modulation of the exchange can relax the Zeeman energy as a second-order effect when an anisotropic interaction mixes spin states of a dimer [32,37,38]. When ions have individual spin $S > 1/2$ the zero-field splitting appears with the Hamiltonian

$$H = JS_1 \cdot S_2 + D\left[S_{iz}^2 - \frac{1}{3}S_i(S_i+1)\right] + E\left(S_i^x S_j^x - S_i^y S_j^y\right) \tag{14}$$

and the anisotropic splitting D and E provide mechanisms of spin–lattice relaxation. The effective relaxation occurs by two-phonon resonance process between states with S differing by 2. The relaxation rate is, however, reduced by factor $(D/J)^2$ as compared to the rate expected from modulation of the isotropic exchange [25].

For ions having $S = 1/2$ the above mechanism is not available. Their place can be taken by another anisotropic interaction as dipolar coupling or g-factor anisotropy. When J is not very small a considerable contribution to anisotropy can arise from anisotropic exchange (pseudo-dipolar coupling) or from antisymmetric exchange $J_{anti}(S_1 \times S_2)$. Modulation of the pseudo-dipolar coupling leads to the resonance two-phonon processes between states for which $\Delta S = \pm 2$, whereas for the antisymmetric perturbation states differing by $\Delta S = \pm 1$ are coupled. The relaxation is generally slower for $S = 1/2$ ions even for large J-values and one can expect a substantial contribution from the Van Vleck mechanism of individual ions.

Quantitative consideration of a two-phonon resonance relaxation process is based on a three-level model and can be specified for any of the above relaxation mechanisms. This model is generally used in a description of the pair relaxation and is presented in Appendix B. The results of spin–lattice relaxation rate calculations with this model (see Eqs. (B3) and (B4)) can be parameterized to the form:

$$\frac{1}{T_{1ferro}} = c|\langle b|V^{(1)}|a\rangle|^2 \frac{J^3}{\exp(J/kT) - 1} \tag{15}$$

for ferromagnetically coupled dimers (Orbach process), and

$$\frac{1}{T_{1antiferro}} = c|\langle b|V^{(1)}|a\rangle|^2 \frac{J^3}{1 - \exp(-J/kT)} \tag{16}$$

for the antiferromagnetic coupling (anti-Orbach process). The squared matrix element should be specified for various relaxation mechanisms. When the isotropic exchange is modulated then $V^{(1)} = r_0(\partial J/\partial r)$, whereas for zero-field splitting modulations $V^{(1)} = r_0(\partial D/\partial r)$ where $r = r_{12}$ is the separation between ions in a dimer and r_0 is its equilibrium value. Generally, the matrix elements are difficult for calculations, but some estimations for Ir^{4+}—Ir^{4+} have been performed [14].

In most cases one can expect that the spin relaxation can be influenced by crystal imperfections or a local disorder around a paramagnetic center. It is well known that the zero-field splitting parameter always displays some distribution. Also r_{12} cannot be identical for all pairs in a crystal. Thus, the relaxation rates should

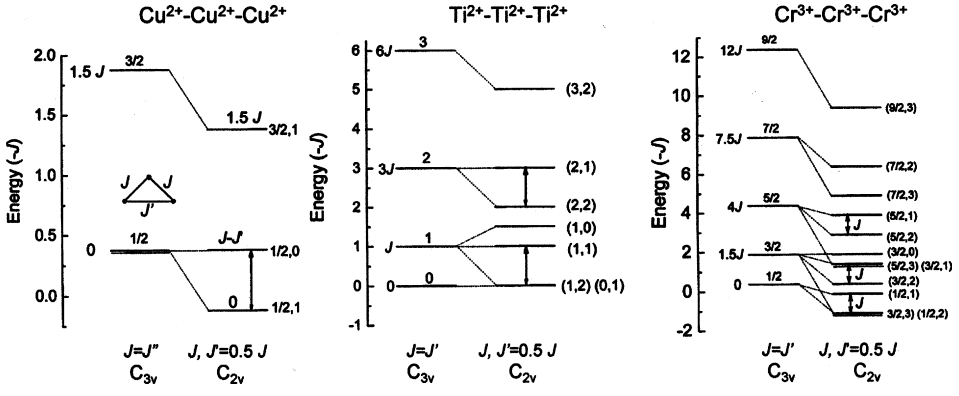

Fig. 6. Energy levels of high symmetry regular triangle triads Cu^{2+}—Cu^{2+}—Cu^{2+} ($S = 3/2$), Ti^{2+}—$Ti^{2+}Ti^{2+}$ ($S = 3$) and Cr^{3+}—Cr^{3+}—Cr^{3+} ($S = 9/2$). The allowed exchange induced transitions are shown by arrows. The energy levels are described in parentheses as (S, S'), where $S' = S_1 + S_2$, and $S = S' + S_3$.

be integrated over a distribution of r_{12} or a distribution of J [39–41] and then the rate can be calculated as

$$\frac{1}{T_1} = B\int_{J_{\min}}^{J_{\max}} \frac{J^3}{\exp(J/kT)-1} r^2 \frac{\mathrm{d}r}{\mathrm{d}J}\mathrm{d}J \tag{17}$$

Assuming the exponential decay of the exchange coupling with interionic distance $J = J_0\exp(-\lambda r)$ we have

$$\frac{1}{T_1} = B\int_{J_{\min}}^{J_{\max}} \frac{[J\ln(J/J_0)]^2}{\exp(J/kT)-1}\mathrm{d}J \tag{18}$$

which leads to a quadratic temperature dependence for $J \ll kT$, as it was reported for irradiated polyethylene [42] and for iron pairs in ferrodoxin [36].

3.3.4. Cross-relaxation between individual ions and spin clusters

Pairs of ions in magnetically diluted dielectric materials always coexist with more numerous individual ions. In such a case the cross-relaxation can appear. The cross-relaxation is a flip–flop process with downward transition of the single ion spin and simultaneous upward transition within the triples state of a pair with subsequent spin–lattice relaxation of the pair. General discussion of the spin relaxation in such a case has been published [43].

The effective relaxation rate depends on the ratio of $(1/T_1)^{\text{pair}}$ to $(1/T_1)^{\text{cross}}$. When the effectiveness of the relaxation path is limited by the pair–lattice relaxation rate the system relaxes with rate proportional to the $(1/T_1)^{\text{pair}}$ and temperature dependence of the relaxation rate via fast cross-relaxation to the slower relaxing pairs is

$$\frac{1}{T_1} = A_{\text{pair}} J^3 \operatorname{cosech}\left(\frac{J}{kT}\right) \tag{19}$$

At high temperatures, when $kT \gg J$ this dependence becomes linear $1/T_1 \propto T$.

When the relaxation path is limited by cross-relaxation rate, the effective relaxation rate is proportional to the cross-relaxation rate $(1/T_1)_{\text{eff}} = \left[N_{\text{pair}}^{\text{triplet}}/N_{\text{rad}}\right](1/T_1)^{\text{cross}}$ and the temperature dependence of the effective relaxation rate via slow cross-relaxation to the fast relaxing antiferromagnetically coupled pairs is

$$\frac{1}{T_1} = A_{\text{cross}}\frac{1}{1+\exp(J/kT)} \tag{20}$$

where A_{cross} is an effective coefficient and J being the singlet–triplet splitting. This dependence is very strong at low temperatures but for $kT \gg J$ the rate becomes temperature independent. Cross-relaxation to pairs described by Eq. (20) was observed for iron ions in borate glasses [44] and for free radicals in disulfide oligomeric system [45], whereas the cross-relaxation described by Eq. (19) was observed for Yb^{3+} in SrF_2 crystal [11].

3.4. Spin–lattice relaxation results for Ti^{2+}—Ti^{2+} pairs in SrF_2

In our research the relaxation rate was found to be practically the same for each of the dimer lines, thus we performed detailed pulsed EPR measurements on the line marked by the asterisk in Fig. 2, which is a superposition of the three dimer lines and therefore it gives a strong electron spin echo signal. The magnetization recovery, monitored by the echo amplitude, is single exponential indicating that the relaxation is described by single relaxation time in the multilevel spin system. It can appear when the spin system achieves the spin temperature during spin relaxation measurements. In fact, the spin–spin relaxation time T_2 and dephasing time T_M are much shorter than the spin–lattice relaxation time T_1 in the measured temperature range and the equilibrium within the spin system is quickly achieved.

Spin–lattice relaxation of the titanium ion pairs in SrF_2 is much faster than the relaxation of individual Ti^{2+} ions (Fig. 5). This suggests that the exchange interaction can contribute to the relaxation via crystal field modulation (zero-field splitting D), via anisotropic exchange which produce transitions between spin states for which $\Delta S = \pm 2$, or via anisotropic exchange which couples states for which $\Delta S = \pm 1$. The possible 14 up-down transitions induced by the anisotropic interactions and involved in the resonance two-phonon (Orbach-type) relaxation processes are shown in Fig. 7. Calculations of the relaxation time require solving master equations for changes in the level populations under action of perturbations producing inter-level transitions. The equation describing the change in the population N_i of the ith level has the form

$$\frac{\mathrm{d}N_i}{\mathrm{d}t} = \sum_j (-W_{ij}N_i + W_{ji}N_j) \tag{21}$$

where W_{ij} is the total probability of transition between ith and jth level and the sum is taken over all allowed transitions ($\Delta S = \pm 1, \pm 2$). Only transition between the two lowest states ($-2 \leftrightarrow -1$) was excited during relaxation measurements as marked in the Fig. 7. The direct two-phonon relaxation, i.e. transitions from $|-1\rangle$ to $|-2\rangle$ is produced by an upward transition "a" ($-1 \leftrightarrow +1$) followed by the "b" ($0 \leftrightarrow -2$) transition and by the pair of transitions $a'b'$ marked in Fig. 7, but all the other transitions are also involved in returning of the spin system to Boltzmann thermal equilibrium.

A general solution of Eq. (21), i.e. explicit expression for $\mathrm{d}(N_{-1} - N_{-2})/\mathrm{d}t$ is not known and detailed calculations were performed up to four-level systems only [46,47]. For higher multilevel systems a simplified three-level model is usually applied. In our case we can neglect the relaxation via upper singlet state $|0\rangle$ where only four up-down transitions are involved compared to the 10 transitions between the two other spin states. Considering the two lowest Zeeman levels only and treating the $S = 1$ states as single state separated by $2J$ from the ground state doublet we have the three-level model which is described in Appendix B. In fact,

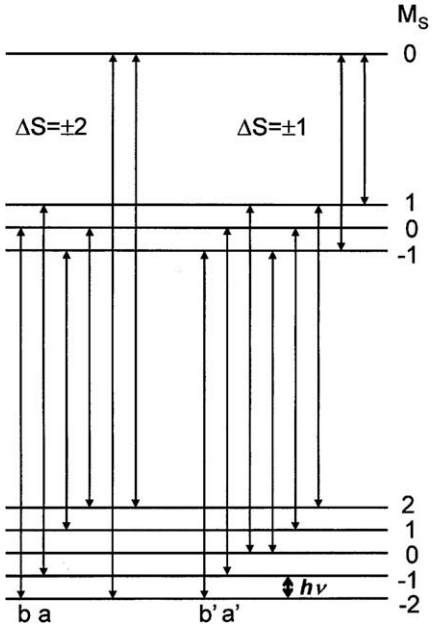

Fig. 7. Energy level diagram of Ti^{2+}—Ti^{2+} pair with transition allowed by zero-field splitting modulations and anisotropic exchange with $\Delta S = \pm 2$, and by anisotropic exchange with $\Delta S = \pm 1$. The a, b and a', b' transitions give direct contribution to the two-phonon Orbach mechanism of spin relaxation between the lowest Zeeman doublet.

the temperature dependence of $1/T_1$ (see Fig. 5) is well described by the following equation

$$\frac{1}{T_1} = a + \frac{b}{\exp(\Delta/kT) - 1} \tag{22}$$

as it is expected for the three-level system with $\Delta = 2J$. The values of parameter of Eq. (22) were obtained by a computer fit to the experimental points (full circles in Fig. 5). The temperature independent term $a = 8500\ \mathrm{cm}^{-1}$ has the same origin as in the case of a single ion relaxation (see Eq. (3)). The second term with $b = 4.9 \times 10^7\ \mathrm{s}^{-1}$ and $\Delta = 72\ \mathrm{cm}^{-1}$ describes Orbach-type relaxation via excited state of energy $2J$ as expected for ferromagnetically coupled pairs (see Eq. (15)). Thus, the ferromagnetic exchange integral is equal to $J = 36\ \mathrm{cm}^{-1}$ and is comparable to the exchange coupling in Cu^{2+}—Cu^{2+} pairs in BaF_2 where $J = 35\ \mathrm{cm}^{-1}$, although the coupling is antiferromagnetic in the Cu^{2+} pair [8].

The relaxation rate of the titanium pairs was measurable up to 30 K only. At this temperature the spin–lattice relaxation rate becomes comparable to the phase relaxation rate and contributes strongly to the electron spin echo dephasing. As a result the EPR lines become progressively homogeneously broadened and electron spin echo signal cannot be observed because the electron spin echo dephasing is so fast that the echo signal falls into the dead time of the spectrometer.

Table 2
Spin–lattice relaxation parameters of ionic pairs in crystals. $H_{ex} = J|S_1 \cdot S_2$ is the exchange Hamiltonian. The sign in front of $|J|$ refers to ferromagnetic coupling if "+" or to antiferromagnetic coupling if "−".

Compound	Pair parameters Spin–lattice relaxation	Reference
SrF_2	Ti^{2+}—Ti^{2+} $S = 2$, $\lvert J\rvert = 36\ \mathrm{cm}^{-1}$ (ferro), $D = 0.036\ \mathrm{cm}^{-1}$ Electron spin echo-saturation recovery, 4.2–24 K $\frac{1}{T_1} = a + \frac{b}{\exp(\lvert 3J\rvert/kT)-1}$, $a = 8500\ \mathrm{s}^{-1}$, $b = 4.9 \times 10^7\ \mathrm{s}^{-1}$	This paper
BaF_2	Cu^{2+}—Cu^{2+} $S = 1$, $\lvert J\rvert = 35\ \mathrm{cm}^{-1}$ (antiferro), $D = 0.0365\ \mathrm{cm}^{-1}$ Electron spin echo-saturation recovery, 4.2–30 K $\frac{1}{T_1} = a + c\left(\frac{T^9}{\Theta_D^{10}}\right) I_8(\Theta_D/T) + d \cdot csch^2\left(\frac{\Delta}{2kT}\right)$, $a = 100\ \mathrm{s}^{-1}$, $c = 1 \times 10^{-10}\ \mathrm{s}^{-1}\ \mathrm{K}$, $\Theta_D = 286\ \mathrm{K}$, $d = 5.5 \times 10^5\ \mathrm{S}^{-1}$, $\Delta = 44\ \mathrm{cm}^{-1}$	[8]
$Zn(detc)_2$	Cu^{2+}—Cu^{2+} $S = 1$, $\lvert J\rvert = 13\ \mathrm{cm}^{-1}$ (ferro), $D = 0.0276\ \mathrm{cm}^{-1}$ Pulse (2 μs–100 ms) saturation recovery EPR, 1.5–25 K $\frac{1}{T_1} = aT + \frac{b}{\exp(\lvert J\rvert/kT)-1}$, $a = 140\ \mathrm{s}^{-1}\ \mathrm{K}^{-1}$, $b = 1.9 \times 10^4\ \mathrm{s}^{-1}$	[12]
Al_2O_3	Cr^{3+}—Cr^{3+} $S = 3$, $\lvert J\rvert = 0.5\ \mathrm{cm}^{-1}$ (antiferro), $D = 0.2\ \mathrm{cm}^{-1}$ Pulse saturation recovery EPR, 1.5–60 K $\frac{1}{T_1} = \frac{b}{1-\exp(-\lvert 5J\rvert/kT)} + cT^7$, $b = 150\ \mathrm{s}^{-1}$, $c = 6 \times 10^{-7}\ \mathrm{s}^{-1}\ \mathrm{K}^{-7}$	[13]
$(NH_4)_2PtCl_6$	Ir^{4+}—Ir^{4+} $S = 3$, $\lvert J\rvert = 5.2\ \mathrm{cm}^{-1}$ (antiferro), $D = 0.42\ \mathrm{cm}^{-1}$ Pulse saturation recovery EPR, 1.5–6 K $\frac{1}{T_1} = \frac{b}{1-\exp(-\lvert J\rvert/kT)}$, $b = 700\ \mathrm{s}^{-1}$	[14]
(2Fe–2S) ferrodoxin	Fe^{3+}—Fe^{2+} $S(5/2+2)$, $\lvert J\rvert = 166\ \mathrm{cm}^{-1}$ (antiferro) Pulse saturation recovery EPR, 1–100 K $\frac{1}{T_1} = aT^2 + cT^9 I_8(\Theta_D/T) + d \cdot \exp\left(-\frac{\Delta}{kT}\right)$, $a = 0.9\ \mathrm{s}^{-1}\ \mathrm{K}^{-2}$, $c = 3.5 \times 10^{-10}\ \mathrm{s}^{-1}\ \mathrm{K}^{-9}$, $\Theta_D = 60\ \mathrm{K}$, $d = 7.3 \times 10^{10}\ \mathrm{s}^{-1}$, $\Delta = 243\ \mathrm{cm}^{-1}$	[36]

Our experimental measurements results are collected in Table 2 together with data published for various dimers in crystals, and corresponding temperature dependencies of $1/T_1$ are plotted in Fig. 8. The results show that in the most cases the modulation of exchange coupling gives the dominant contribution to the spin–lattice relaxation consistent with theoretical predictions for ferro- and antiferro coupling. The relaxation at low temperatures is generally faster for ferromagnetic-type coupling with b-coefficient order of 10^4—$10^7\ \mathrm{s}^{-1}$, and is slower for antiferromagnetic coupling, where b is order of 150—700 s^{-1}. This reflects a difference in thermal population of the Zeeman levels and in effectiveness of the relaxation mechanism described by the squared matrix element $|\langle b|V^{(1)}|a\rangle|^2$. For some antiferromagnetically coupled dimers, even having large J-values (Cu^{2+}—Cu^{2+} in BaF_2 and Fe^{3+}—Fe^{2+} in ferrodoxin) the exchange relaxation mechanism is dominated by ordinary Raman processes of individual ions. For the iron dimers in ferrodoxin the exchange coupling contribution to the relaxation is given by the first term aT^2 (see Table 2) as expected for a distribution of the relaxation times in a biological material.

Relatively large temperature independent contribution (term a in Eq. (22)), arising from cross-relaxation, exists for titanium(II) and copper(II) dimers in fluorites. It is consistent with known tendency of clusterization of ions in the fluorite structures. It should be noted that most relaxation measurements were performed at low temperatures, thus the relaxation processes which become effective at higher temperatures were not visible. The measurements for Cr^{3+}-dimers and Ir^{4+}-dimers performed in the 60 s were relatively of low accuracy, but they deliver a good background for an elaboration of relaxation theories.

Measurements of pair relaxation are always accompanied by measurements of individual ion relaxation. The results are compared in Fig. 9. They confirm an opinion that when pair relaxation is governed by modulations of exchange interaction then pairs relax faster than individual ions at least at low temperatures, although for Cu^{2+} relaxation rate of pairs and individual ions becomes comparable at temperature higher than 30 K. When this mechanism does not contribute to a relaxation, as it is for Cu^{2+} ions in BaF_2, the individual ions relax faster than the dimers.

3.5. Electron spin echo dephasing (phase relaxation) and ESEEM spectrum

The phase relaxation called electron spin echo dephasing is a much less explored field as compared to the spin–lattice relaxation. The phase relaxation is a random process of decoherence of the precession motion of spins excited by microwave pulses lead-

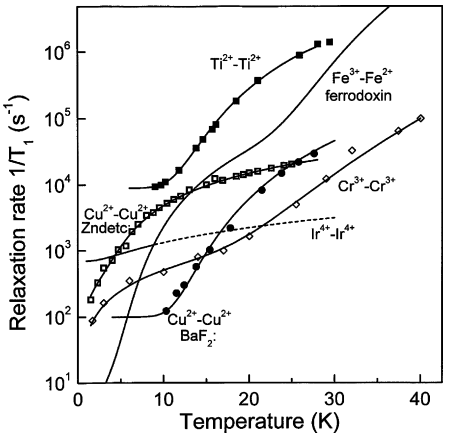

Fig. 8. Temperature dependence of the spin–lattice relaxation rate for ionic pairs in crystals according to the data collected in Table 2.

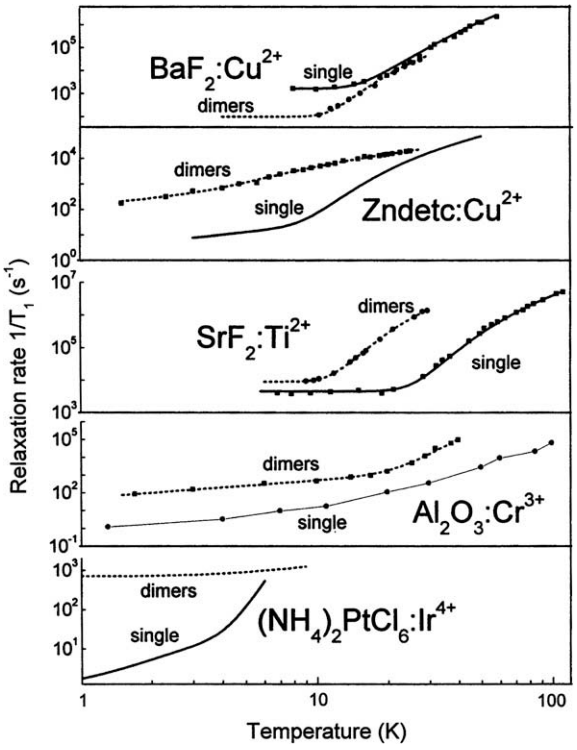

Fig. 9. Comparison of relaxation rate $1/T_1$ for individual ions and their pairs in solids.

ing to the final precession with random phases. This is observed as a decay of two-pulse electron spin echo (ESE) signal amplitude V with time after excitation. The decay is characterized by the phase memory time T_M. The decay can be produced by various mechanisms [48–50] and can be described as $V(\tau) = V_0 \cdot \prod_k \exp(-a_k \tau^k)$, where $k = 0.5-3$ depending on the dephasing mechanism, and τ is an interval between exciting and refocusing pulse. The T_M is well defined for a single exponential decay function $V_{decay}(2\tau) = V_0 \exp(-2\tau/T_M)$. In general, for a single exponential decay the T_M can be defined as $T_M = (1/a_k)^{1/k}$. For Ti^{2+} and titanium pairs in SrF_2 the decay is single exponential and the dephasing rate $1/T_M$ varies with temperature as it is presented in Fig. 5.

A single exponential ESE decay with $k = 1$ can arise from instantaneous diffusion (ID), by spin–lattice relaxation processes and by molecular motions. Only the first and the second phenomenon contributes to the decay in SrF_2. The observed temperature dependence of the $1/T_M$ for individual ions as well as for pairs is shown in Fig. 5 and is well described as

$$\frac{1}{T_M} = \left(\frac{1}{T_M}\right)_0 + \frac{1}{T_1(T)} \tag{23}$$

with temperature independent ID-contribution $(1/T_M)_0 = 1.1 \times 10^6\ s^{-1}$ for single Ti^{2+} ions and $(1/T_M)_0 = 0.75 \times 10^6\ s^{-1}$ for Ti^{2+}—Ti^{2+} pairs. This contribution is typical for the ID mechanism produced by the refocusing pulse and arises from dipolar coupling between excited spins forming echo signal [49,50]. Because number of individual ions is larger than the number of pairs the dephasing rate $(1/T_M)_0$ is higher for single ions.

Two-pulse electron spin echo decay was strongly modulated both for the single ions and the pairs as it is presented for $T = 9$ K in Fig. 10. The modulations are produced by a weak dipolar coupling with surrounding magnetic nuclei. Fourier Transform of the modulation function gives pseudo-ENDOR spectra (ESEEM spectra) with peaks at Larmor frequencies of modulating nuclei

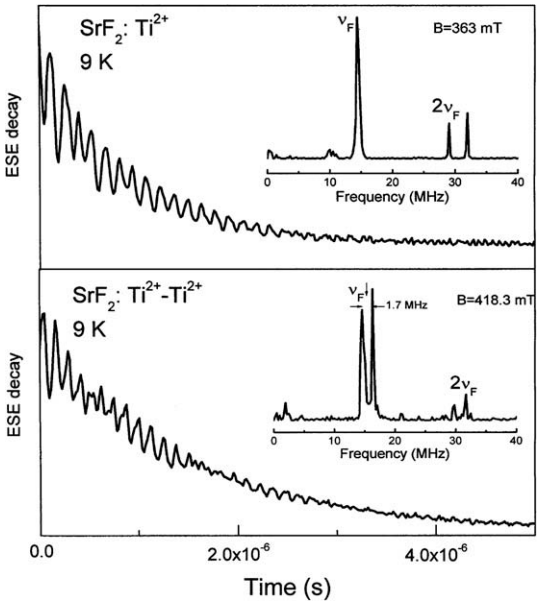

Fig. 10. Modulated two-pulse electron spin echo decay for Ti^{2+} and Ti^{2+}—Ti^{2+} pairs in SrF_2 at 9 K. The insets show the ESEEM spectra being the Fourier transforms of the modulation function.

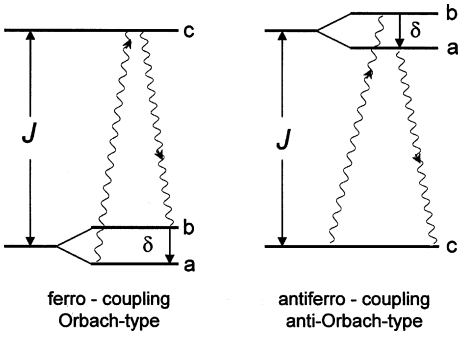

Fig. 11. The three-level model used in calculations of the two-phonon resonance relaxation process of Zeeman doublet a, b (having splitting δ) via singlet state c split by exchange interaction J. Phonon excitations are shown by the waving lines.

and at their harmonics. The spectra are shown as insets in Fig. 10. The peaks appear at frequency ν_F of ^{19}F nuclei and at $2\nu_F$. The modulations are expected from ^{19}F nuclei at distances in the range 0.25–0.5 nm, whereas closely located fluorine nuclei give a weak unresolved superhyperfine structure within the EPR line. Therefore, the single peak at ν_F from monomeric Ti^{2+} located in the center of the fluorine cube is due to farther located fluorine atoms (matrix atoms). In ENDOR spectrum of the pairs the peak at ν_F is split into a doublet with splitting $\Delta\nu = 1.7$ MHz. Ti^{2+} ions in pairs are off-center shifted (see Fig. 1) and some fluorine nuclei (located in the rotated plane for upper Ti^{2+} in Fig. 1, and symmetrically for the lower Ti^{2+}) are now in the distance giving dipolar splitting of the lines in the ENDOR spectrum, i.e. they modulate echo decay with two slightly different frequencies. This splitting $\Delta\nu$ has the same value as we measured for the off-center Cu^{2+} ions in BaF_2 [8]. Thus, the off-center shift of Ti^{2+} in dimeric species is approximately the same as that for Jahn–Teller shifted Cu^{2+} in fluorite structure. The off-center shift can be evaluated as 0.13 nm.

4. Conclusions

Electron spin–lattice relaxation is faster for pairs than that for individual Ti^{2+} ions in SrF_2 crystals. Such a situation appears gen-

erally for pairs when spin of ions is $S > 1/2$. It is because the zero-field splitting modulations by phonons are very effective relaxation mechanism in the second order. Orbach-type and anti-Orbach-type temperature dependence produced by this mechanism allows direct determination of the exchange coupling parameter J when a simple three-level model is applicable. We found a ferromagnetic coupling between Ti^{2+} ions with the singlet–triplet splitting $J = 36\ cm^{-1}$. For ions with $S = 1/2$ the spin–phonon the coupling is small and the spin relaxation of such a pair can be dominated by mechanisms characteristic for individual ions.

A very effective mechanism of J modulations produces a rapid increase of the spin–lattice relaxation rate $1/T_1$ with temperature. This spin–lattice relaxation mechanism contributes strongly to the electron spin echo dephasing. As the result the increase of the dephasing rate $1/T_M$ with temperature is entirely due to the spin–lattice relaxation processes of pairs. Fourier transform of the electron spin echo decay modulations due to surrounding ^{19}F nuclei shows dipolar splitting in the ESEEM spectrum. From this splitting value the off-center shift (shift from the center of the TiF_8 cube) of Ti^{2+} in a Ti^{2+}—Ti^{2+} pair was estimated as 0.13 nm.

Appendix A. Transport integral I_6

The transport integral $I_6(\Theta_D/T) = \int_0^{\Theta_D/T} x^6 e^x (e^x - 1)^{-2} dx$ is tabulated in [29], but for numerical applications it can be approximated by

(a) in the range $0.1 < \Theta_D/T < 18.6$

$$I_6 = \exp(P) \tag{A1}$$

where
$P = -1.66685 + 4.86552t - 0.12413t^2 - 0.03392t^3 - 0.02587t^4 - 0.03595t^5 - 0.00527t^6 + (53.9 \times 10^{-4})t^7 + (6.40378 \times 10^{-4})t^8 - 28.51 \times 10^{-5})t^9$, and $t = \ln(\Theta_D/T)$

(b) in the range $18.6 < \Theta_D/T < 30$

$$I_6 = 732.48735 - 0.18479 * \exp(-(r - 18.6)/1.37037) \tag{A2}$$

where $r = \Theta_D/T$.

Appendix B. Three-level model of electron spin–lattice relaxation of dimers

Quantitative considerations of a two-phonon resonance relaxation process are based on a simple three-level model. In a multilevel case one can consider relaxation of a Zeeman doublet via single excited state coupled by an exchange interaction. In this approach the thermal equilibrium within the spin system is assumed and it is described by the spin temperature. Then the multilevel spin system relaxes with a single relaxation time. The three-level systems for a ferro and antiferro-coupled case are shown in Fig. 11 where the phonon transitions accompanying the relaxation spin-flops are shown by waving lines.

Relaxation time of the system can be calculated from the probability of transitions between states a, b, c induced by perturbation being a lattice vibration. The probability of transition between two electron state m, n differing in energy of Δ and accompanied by simultaneous creation of phonon can be calculated for the periodic H' perturbation from the Fermi golden rule

$$w_{mn} = \frac{2\pi}{\hbar} |\langle m, \bar{n}|H'|n, \bar{n}+1\rangle|^2 \rho(\omega) \tag{B1}$$

where $\bar{n} = \left[\exp\left(\frac{\Delta}{kT}\right) - 1\right]^{-1}$ is phonon occupation number and $\rho(\omega)$ is the density of the phonon states which for Debye model is $\rho(\omega) = 3V\omega^2/(2\pi v^3)$ for unit crystal volume V and v is the sound velocity. For perturbation of the form $H' = \varepsilon V^{(1)}$ (see Eq. (4)), where ε is the strain produced by phonons, one can separate the matrix elements $\langle m, \bar{n}|H'|n, \bar{n}+1\rangle = \langle m|V^{(1)}|n\rangle\langle\bar{n}|\varepsilon|\bar{n}+1\rangle$ and $|\langle\bar{n}|\varepsilon|\bar{n}+1\rangle|^2 = \frac{\hbar\omega}{2Mv^2}(\bar{n}+1)$ where M is the mass of the crystal. Thus, the probability of transition between spin states split by $J = \hbar\omega$ with creation of phonon is

$$w_{mn} = \frac{3J^3}{2\pi\rho v^5\hbar^4} |\langle m|V^{(1)}|n\rangle|^2 (\bar{n}+1) = B(\bar{n}+1) \tag{B2}$$

For the opposite transition accompanied by the phonon annihilation $w_{nm} = B\bar{n}$.

Probabilities of transitions between levels of the three-level system with doublet states lower (ferromagnetic coupling) (Fig. 11) are $w_{bc} = w_{ac} = B \cdot \bar{n}$ and $w_{cb} = w_{ca} = B \cdot (\bar{n}+1)$ when $\delta \ll kT$ and $\delta \ll J$. In a similar way one can calculate transition probabilities for the case of antiferromagnetic coupling when the singlet level is lower. The relaxation rates $1/T_1$ calculated from the rate equations governing the level populations are simply proportional to the density of phonons in the final state, i.e. $1/T_{1ferro} = B \cdot \bar{n}$ and $1/T_{1antiferro} = B \cdot (\bar{n}+1)$. Thus, for ferromagnetic coupling the ordinary expression for the Orbach-type relaxation process is obtained

$$\frac{1}{T_{1ferro}} = \frac{3}{2\pi\rho v^5\hbar^4} \frac{J^3}{\exp(J/kT) - 1} |\langle b|V^{(1)}|a\rangle|^2 \tag{B3}$$

and for the antiferromagnetic coupling (anti-Orbach process)

$$\frac{1}{T_{1antiferro}} = \frac{3}{2\pi\rho v^5\hbar^4} \frac{J^3}{1 - \exp(-J/kT)} |\langle b|V^{(1)}|a\rangle|^2 \tag{B4}$$

The squared matrix element should be specified for various relaxation mechanisms described by appropriate perturbation Hamiltonians.

References

[1] M.W. Makinen, G.B. Wells, Application of EPR saturation methods in paramagnetic metal ions in proteins, in: H. Sigel (Ed.), Metal Ions in Biological Systems, Marcel Dekker, New York, 1987, pp. 129–206.
[2] I. Moura, A. Macedo, J.J.G. Moura, EPR of iron–sulfur and mixed-metal clusters in proteins, in: A.J. Hoff (Ed.), Advanced EPR. Applications in Biology and Biochemistry, Elsevier, Amsterdam, 1989, pp. 813–838.
[3] D.J. Hirsh, G.W. Brudvig, Long-range electron spin–spin interactions in the bacterial photosynthetic reaction center, J. Phys. Chem. 97 (1993) 13216–13222.
[4] S.A. Dzuba, A. Kawamori, N. Katsuta, H. Hara, H. Mino, S. Itoh, Spin relaxation of a spin-correlated radical pair $P_{700}^{+}A_1^{-}$ in the PSI photosynthetic reaction center, Chem. Phys. Lett. 362 (2002) 307–313.
[5] T.S. Lin, Electron spin echo spectroscopy of organic triplets, Chem. Rev. 84 (1984) 1–15.
[6] J.B. Horak, A.W. Nolle, Electronic and nuclear relaxation in crystals with fluorite structure containing Eu^{2+} or Mn^{2+}, Phys. Rev. 153 (1967) 372–378.
[7] R.L. Garrifulina, V.G. Stiepanov, Exchange-coupled pair of Mn^{2+} ions in CaF_2 and SrF_2, Fiz. Tverd. Tela 15 (1973) 2169–2172.
[8] S.K. Hoffmann, J. Goslar, S. Lijewski, V.A. Ulanov, Molecular structure and dynamics of off-center Cu^{2+} ions and strongly coupled Cu^{2+}—Cu^{2+} pairs in BaF_2 crystals: electron paramagnetic resonance and electron spin relaxation studies, J. Chem. Phys. 127 (2007) 144705, 1–13.
[9] M.M. Zaripov, V.S. Kropotov, L.D. Livanova, V.G. Stiepanov, EPR of copper and titanium ions in CaF_2, Fiz. Tverd. Tela 9 (1967) 2985.
[10] I.I. Fazlishanov, V.A. Ulanov, M.M. Zaripov, R.M. Eremina, Local structure of dimeric titanium centers in SrF_2 crystals studied by EPR and ENDOR, Fiz. Tverd. Tela 44 (2002) 1483–1486.
[11] M. Velter-Stefanescu, V. Nistor, V.V. Grecu, Exchange-coupled pairs of Yb^{3+} ions in SrF_2, Phys. Rev. B 34 (1986) 1459–1466.
[12] S.A. Altshuler, R. Kirmse, B.V. Solovev, Spin–lattice relaxation of exchange-coupled Cu^{2+}—Cu^{2+} pairs and single Cu^{2+} ions in crystals of zinc(II)bis(diethyldithiocarbamate), J. Phys. C: Solid State Phys. 8 (1975) 1907–1920.
[13] J.C. Gill, Spin–lattice relaxation of chromium ions in ruby, Proc. Phys. Soc. (London) 79 (1962) 58–68.
[14] E.A. Harris, K.S. Yngvesson, Spin–lattice relaxation in some iridium salts: II. Relaxation of nearest-neighbour exchange-coupled pairs, J. Phys. C (Proc. Phys. Soc.) 1 (2) (1968) 1011–1023.

[15] S.K. Hoffmann, V.A. Ulanov, Off-centre dynamic Jahn–Teller effect studied by electron spin relaxation of Cu^{2+} ions in SrF_2 crystal, J. Phys.: Condens. Matter 12 (2000) 1855–1866.
[16] V.A. Ulanov, M. Krupski, S.K. Hoffmann, M.M. Zaripov, Effects of hydrostatic pressure and temperature on the electron paramagnetic resonance spectrum of off-centre Jahn–Teller $[CuF_4F_4]$ complexes in SrF_2 crystal, J. Phys.: Condens. Matter 15 (2003) 1081–1096.
[17] M. Moreno, M.T. Barriuso, J.A. Aramburu, P. Garcia-Fernandez, J.M. Garcia-Lastra, Microscopic insight into properties and electronic instabilities of impurities in cubic and lower symmetry insulators: the influence of pressure, J. Phys.: Condens. Matter 18 (2006) R315–R360.
[18] M.M. Zaripov, V.S. Kropotov, L.D. Livanova, V.G. Stiepanov, EPR spectra of Ti^{2+} in SrF_2 and Cu^{2+} in CdF_2, Fiz. Tverd. Tela 10 (1968) 34–38.
[19] J.R. Herrington, T.L. Estle, EPR investigation of Ti^{2+} in SrF_2 single crystal, J. Chem. Phys. 57 (1972) 3571–3572.
[20] M.M. Zaripov, Yu.F. Mitrofanov, Yu.E. Polskyi, M.L. Falin, ENDOR investigation of iron group ions in homological series of fluorite-type crystals, in: S.A. Altshuler (Ed.), Paramagnitnyj Riezonans, vol. 8–9, Izd. Kazanskogo Universiteta, 1974, pp. 163–201.
[21] M.K. Bowman, Electron spin–lattice relaxation in nonionic solids, in: L. Kevan, R.N. Schwartz (Eds.), Time Domain Electron Spin Resonance, J. Wiley, New York, 1979, pp. 67–106.
[22] S.S. Eaton, G.R. Eaton, Relaxation times of organic radicals and transition metal ions, in: L.J. Berliner, S.S. Eaton, G.R. Eaton (Eds.), Biological Magnetic Resonance, Distance Measurements in Biological Systems by EPR, vol. 19, Kluwer, New York, 2000, pp. 29–154.
[23] L.T. Ho, D.P. Dandekar, J.C. Ho, Low-temperature heat capacities of SrF_2 and other fluoride compounds, Phys. Rev. B 27 (1983) 3881–3883.
[24] S. Lijewski, J. Goslar, S.K. Hoffmann, Electron spin echo of Cu^{2+} in the triglycine sulfate crystal family (TGS, TGSe, TGFB): electron spin–lattice relaxation, Debye temperature and spin–phonon coupling, J. Phys.: Condens. Matter 18 (2006) 6159–6169.
[25] E.A. Harris, K.S. Yngvesson, Spin–lattice relaxation in some iridium salts: I. Relaxation of the isolated $(IrCl_6)^{2-}$ complex, J. Phys. C (Proc. Phys. Soc.) 1 (2) (1968) 990–1010.
[26] S.K. Hoffmann, W. Hilczer, J. Goslar, M.A. Augustyniak-Jablokow, Raman spin–lattice relaxation, Debye temperature and disorder effects studied with electron spin echo of Cu^{2+} in Tutton salt crystals, J. Phys.: Condens. Matter 13 (2001) 7443–7457.
[27] R.B. Griffiths, Theory of magnetic exchange–lattice relaxation in two organic free radicals, Phys. Rev. 124 (1961) 1023–1030.
[28] P.M. Richards, Correlations in magnetic exchange–lattice relaxation, Phys. Rev. 137 (1965) A1327–A1334.
[29] W.M. Rogers, R.L. Powell, Tables of transport integrals, Natl. Bur. Stand. Circ. (U.S.) 1 (1958) 1–55.
[30] S.K. Hoffmann, W. Hilczer, J. Goslar, EPR, electron spin–lattice relaxation, and Debye temperature of Cu(II)-doped triglycine selenate crystal, J. Magn. Res. A 122 (1966) 37–41.
[31] S.K. Hoffmann, W. Hilczer, J. Goslar, Weak long-distance superexchange interaction and 1st temperature variation in copper(II) compounds studied by single crystal EPR, Appl. Magn. Res. 7 (1994) 289–321.
[32] A. Bencini, D. Gatteschi, Electron Paramagnetic Resonance of Exchange Coupled Systems, Springer, Berlin, 1990 (Chapter 5).
[33] O. Kahn, Molecular Magnetism, VCH Publ., New York, 1993 (Chapter 10).
[34] C.A. Bates, R.F. Jasper, The properties of exchange-coupled triads of Cr^{3+} ions in ruby, J. Phys. C: Solid State Phys. 4 (1971) 2330–2340.
[35] C.A. Bates, R.F. Jasper, The relaxation of exchange-coupled triads in ruby, J. Phys. C: Solid State Phys. 4 (1971) 2341–2353.
[36] P. Bertrand, J.-P. Gayda, K.K. Rao, Electron spin–lattice relaxation of the (4Fe–4S) ferrodoxin from *B. stearothermophilus*. Comparison with other iron proteins, J. Chem. Phys. 76 (1982) 4715–4719.
[37] J.C. Gill, The establishment of thermal equilibrium in paramagnetic crystals, Rep. Prog. Phys. 38 (1975) 91–150.
[38] J. Owen, E.A. Harris, Pair spectra and exchange interactions, in: S. Geschind (Ed.), Electron Paramagnetic Resonance, Plenum, New York, 1972 (Chapter 6).
[39] S.A. Altshuler, The mechanisms of paramagnetic spin-lattice relaxation in ionic crystals at low temperatures, J. Exp. Theor. Phys. (Russ.) 43 (1962) 2318–2319.
[40] L.R. Dalton, A.L. Kwiram, J.A. Cowen, Electron spin–lattice relaxation in molecular crystals: $S = 1/2$, Chem. Phys. Lett. 17 (1972) 495–499.
[41] S.K. Misra, Spin–lattice relaxation times in amorphous materials as effected by exchange interaction, tunneling level states (TLS) centres, and fractions, Spectrochim. Acta A 54 (1998) 2257–2267.
[42] L.Ya. Djavaghishvili, G.D. Ketiladze, T.I. Sanadze, EPR spectrum and spin–lattice relaxation of irradiated polyethylene, Fiz. Tverd. Tela (Russ.) 10 (1968) 3715–3717.
[43] M.B. Schulz, C.D. Jeffries, Spin–lattice relaxation of rare-earth ions in LaF_3, Phys. Rev. 149 (1966) 270–288.
[44] P.K. Zinsou, D. Vergnoux, G. Ablard, J. Pescia, S.K. Misra, R. Berger, Temperature and concentration dependences of the spin–lattice relaxation rate in four borate glasses doped with Fe_2O_3, Appl. Magn. Res. 11 (1996) 487–492.
[45] S.K. Hoffmann, W. Hilczer, J. Goslar, S. Kiczka, I. Polus, Resonance-type effects in free radical electron spin–lattice relaxation and electron spin echo dephasing due to a dynamics of a homogeneous-chain oligomeric system, Phys. Chem. Chem. Phys. 4 (2002) 4944–4951.
[46] H. Shikata, A phenomenological description of electron paramagnetic double-resonance relaxation of organic free radicals in solution: I. Theory of ENDOR based on the spin-population number method, Bull. Chem. Soc. Jpn. 50 (1977) 3084–3089.
[47] R.Kh. Sabirov, Multiphonon processes in nuclear relaxation via paramagnetic centers, Radiophys. Quantum Electron. 38 (1995) 698–701.
[48] S.K. Hoffmann, J. Goslar, W. Hilczer, M.A. Augustyniak-Jablokow, S. Kiczka, Dephasing relaxation of the electron spin echo of the vibronic $Cu(H_2O)_6$ complexes in Tutton salt crystals at low temperatures, J. Magn. Res. 153 (2001) 56–68.
[49] K.M. Salikhov, A.G. Semenov, Yu.D. Tsvetkov, Electron Spin Echo and its Application (Russ.), Nauka, Novosibirsk, 1976.
[50] K.M. Salikhov, S.A. Dzuba, A.M. Raitsimring, The theory of electron spin-echo signal decay resulting from dipole–dipole interactions between paramagnetic centers in solids, J. Magn. Res. 42 (1981) 255–276.